Magn Reson Med Sci 2021; 20; 99–105
doi:10.2463/mrms.tn.2019-0081
Published Online: March 6, 2020

TECHNICAL NOTE

Accelerated Acquisition of High-resolution Diffusion-weighted Imaging of the Brain with a Multi-shot Echo-planar Sequence: Deep-learning-based Denoising

Motohide Kawamura, Daiki Tamada*, Satoshi Funayama, Marie-Luise Kromrey, Shintaro Ichikawa, Hiroshi Onishi, and Utaroh Motosugi

To accelerate high-resolution diffusion-weighted imaging with a multi-shot echo-planar sequence, we propose an approach based on reduced averaging and deep learning. Denoising convolutional neural networks can reduce amplified noise without requiring extensive averaging, enabling shorter scan times and high image quality. The preliminary experimental results demonstrate the superior performance of the proposed denoising method over state-of-the-art methods such as the widely used block-matching and 3D filtering.

Keywords: *magnetic resonance imaging, diffusion weighted imaging, deep learning, multi-shot echo-planar imaging*

Introduction

Diffusion-weighted MRI (DWI) has been widely used in clinical practice, especially for the early detection of acute stroke.[1] DWI is typically combined with single-shot echo-planar imaging (EPI),[2] which is a fast scanning sequence adequate for avoiding motion-induced artifacts. Despite the short scan times, single-shot EPI can retrieve susceptibility artifacts, image distortion at tissue–air interfaces, and T_2^* blurring, thus limiting its spatial resolution.[3] Various image acquisition and reconstruction approaches address limited spatial resolution. Parallel imaging[4,5] is widely used to accelerate *k*-space traversal along the phase-encoding direction and suppress image distortion. *k*-Space traversal times have been further reduced by using multi-shot techniques including navigator-based reacquisition[6] and multiplexed sensitivity encoding,[7] and their combination enable high-resolution DWI with minimum distortion. However, these techniques often suffer from low intrinsic signal-to-noise ratio (SNR). Moreover, multi-shot methods extend acquisition times according to the number of shots covering a full *k*-space. Consequently, improved image quality requires long acquisition times for signal averaging, limiting the clinical use of high-resolution DWI.

Exploiting prior knowledge about magnetic resonance images enables image reconstruction from a reduced amount of data without losing essential information, and deep neural networks could be used to determine underlying data structures.[8] In fact, deep learning allows to efficiently encode and extract useful features from data using network structures, being among the most powerful approaches for solving problems in many fields and providing outstanding performance compared to other methods, as confirmed in several data science competitions.[9,10] Moreover, massive parallel computation on graphics processing units allows neural networks to perform inference faster than other state-of-the-art algorithms, suggesting its suitability for clinical applications. Furthermore, plenty of MRI data available from clinical practice can be used to train deep neural networks and achieve high performance.

This study aimed to accelerate the process of high-resolution multi-shot DWI by replacing the time-consuming acquisition for signal averaging with denoising based on a deep neural network, as illustrated in Fig. 1. During training, the network learns the relationship between low-SNR images without averaging and high-SNR images obtained from averaging. Then, it can infer high-quality images resembling the averaging effect from non-averaged images, notably reducing the scan times required to obtain averaging data. Preliminary results show that the proposed denoising method outperforms conventional algorithms such as total variation (TV) denoising and block-matching and 3D filtering (BM3D) in both image quality measures and subjective visual quality.

Department of Radiology, University of Yamanashi, Yamanashi, Japan

*Corresponding author: Department of Radiology, University of Yamanashi, 1110 Shimokato, Chuo-shi, Yamanashi 409-3898, Japan. Phone: +81-55-273-1111, Fax: +81-55-273-6744, E-mail: dtamada@yamanashi.ac.jp

Received: October 1, 2018 | Accepted: January 20, 2020

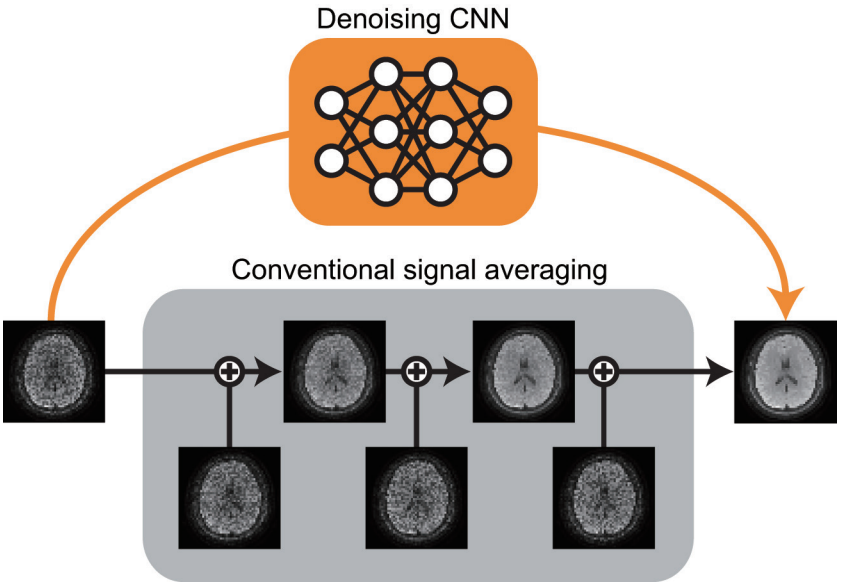

Fig. 1 Schematic of proposed deep-learning-based acceleration for diffusion-weighted imaging (DWI). The conventional approach averages several signals to improve the low signal-to-noise ratio of high-resolution diffusion-weighted images. We replace this time-consuming process with denoising based on deep neural network to notably reduce acquisition time.

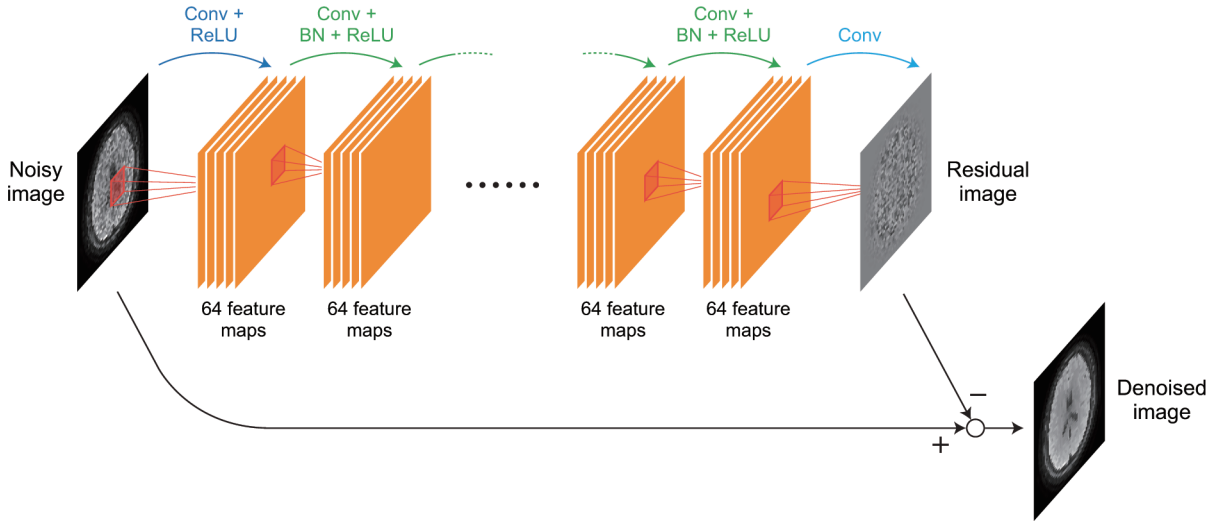

Fig. 2 Architecture of proposed deep convolutional neural network.

Materials and Methods

Data acquisition

This study was approved by the Institutional Review Board. Diffusion-weighted images were acquired from 44 patients and five healthy volunteers (22 men and 27 women; mean age 60.1 years; range 12–87 years) on a 3T MRI scanner (SIGNA Premier, GE Healthcare, Chicago, IL, USA) using a 48-channel head coil in November and December 2018. For each subject, 25–27 axial slices of the brain with thickness of 5 mm were acquired using EPI sequence. Motion probing gradient were applied along the *X*, *Y* and *Z* axes. To acquire less distorted high-resolution images, two-shot multiplexed sensitivity encoding was used along with parallel imaging with reduction factor of 2 using TR and TE of 5000 and 74 ms, respectively. The matrix size was 320 × 320, and the final resolution was 512 × 512 by upscaling during reconstruction. For b = 1000 s/mm^2, the number of excitations (NEX) was 10. For b = 0 s/mm^2, no averaging was performed (i.e., NEX 1). To evaluate the process acceleration, we measured the acquisition time using NEX 1 for both b of 1000 and 0 s/mm^2. This evaluation corresponds to a clinical situation where deep learning is applied instead of signal averaging. No image from this scan was used for training, validation or test of the neural network.

Neural network architecture

We adopt the deep convolutional neural network (CNN) proposed by Zhang et al.[11] for denoising diffusion-weighted images. The network consists of three types of layers as shown in Fig. 2. The input layer contains 64 filters with 3 × 3 windows for convolution followed by rectified linear units to

handle nonlinearity, resulting in 64 feature maps. For each intermediate layer, the feature maps are convoluted by 64 filters with 3 × 3 × 64 windows, followed by batch normalization and rectified linear units. Finally, the output layer has a filter with 3 × 3 × 64 windows that retrieve the denoised image. Throughout the layers, zero padding for convolution preserves the image size. Besides the CNN, we use a residual learning strategy[10] for extracting the noise from a pre-denoising image rather than to directly learn the mapping from the pre-denoising image to a latent clean image. The CNN was only applied to magnitude images, and no complex image was used at any stage. The proposed two-dimensional image denoising applied every process on each slice but not on the whole slices.

Network training and evaluation

Data from the 49 subjects were acquired using NEX 10 and b = 1000 s/mm^2 and divided into three groups comprising training, validation, and test sets. Specifically, data from 24 subjects were used for training, from other six for validation, and from the remaining 19 for test. The images with NEX 9, corresponding to a ninefold signal averaging, were regarded as ground truth and images with NEX 1 as pre-denoising images. The target residual image was defined from these two images. We used 624 input-target pairs of images with size 512 × 512 for training. Bicubic interpolation with enlargement factors of 0.9, 0.8 and 0.7 was applied to the images for data augmentation. Using these original and reduced images, we randomly cropped 384,000 patches with size 50 × 50 at the beginning of every epoch and considered the patches as training input. We used the averaged mean squared errors between target and inferred residual images as loss function and performed Adam optimization[12] during training. The mini-batch size was 128. The network depth was set to 20, corresponding to receptive field size of 41 × 41. The learning rate was set to 1.0×10^{-4} for the first 20 epochs and then it was dropped to 1.0×10^{-5} for the rest of the training. Training was terminated based on an early stopping condition to avoid overfitting problem. Early stopping patience is set to 10 epochs. Test data were used to assess the improvement in image quality after denoising. We evaluated the image quality of the diffusion-weighted images (b = 1000 s/mm^2), before and after denoising.

To evaluate the image quality, we compared the proposed method with other denoising algorithms including Gaussian filter, TV denoising,[13] and BM3D.[14] The standard deviation of the Gaussian filter was 1.21. For TV denoising, the split Bregman method[15] was applied to solve the following optimization problem:

$$\min_x TV(x) + \frac{\lambda}{2}\|y - x\|_2^2, \quad (1)$$

where x is the reconstructed image, y is the pre-denoising image, TV(x) denotes the TV penalty, and λ is the regularization parameter, which we set to 9.5. For BM3D, the standard deviation of the noise was estimated as 0.0824. We adjusted the standard deviation of the Gaussian filter, the regularization parameter for TV minimization, and the estimated noise level of BM3D by optimizing the peak SNR on the validation images. In all schemes, images were normalized prior to denoising.

The peak SNR was used as objective image quality measure, and is defined as

$$Peak\ SNR = 10log_{10}\left(\frac{1}{\frac{1}{M \times N}\sum_{i=1}^{M}\sum_{j=1}^{N}[I_{ground\ truth}(i,j) - I_{denoised}(i,j)]^2}\right), \quad (2)$$

where $I_{\text{ground truth}}(i, j)$ and $I_{\text{denoised}}(i, j)$ denote the intensities of ground truth and denoised image with size $M \times N$, respectively. The test set consisted of the data obtained from the 19 subjects. For evaluation, a single slice was selected from each subject following the criteria that the slice includes the horns of both lateral ventricles. Peak SNR was calculated for the original images and also for the images denoised by the proposed, and the conventional denoising methods. Paired t-test was performed to test the null hypotheses that there was no significant difference between a pair of two approaches. The test was separately performed for each comparison. The comparisons were made between all possible pairs of all methods. Bonferroni correction was used to adjust for multiple comparisons.

We also conducted a visual assessment on the diffusion-weighted images with the assistance of two radiologists, who compared our proposed method to TV denoising, BM3D, and the ground-truth images. The assessment was based on preference of diagnostic radiologists. They were asked which image is preferred when they make imaging-based diagnosis. Specifically, we selected the same 19 slices as for the peak SNR evaluation. Every pair of corresponding images were compared side-by-side. Therefore, the radiologists compared 114 pairs of images without knowledge of their denoising type. The comparison of images h and i in each pair was based on a five-point ordinal scale (1: h is much worse than i, 2: h is worse than i, 3: comparable quality, 4: h is better than i, 5: h is much better than i). The two radiologists separately rated the images. The data were analyzed using the cumulative logit model:[16,17]

$$log\left(\frac{P(Y_{hi} \le j)}{1 - P(Y_{hi} \le j)}\right) = \alpha_j - (\mu_h - \mu_i), \ldots j = 1, \cdots, 4, \quad (3)$$

where Y_{hi} denotes the ordinal-scale random variable, α_j are intercept parameters satisfying $\alpha_1 < \alpha_2 < \alpha_3 = -\alpha_2 < \alpha_4 = -\alpha_1$, and μ_h and μ_i represent the quality of images h and i, respectively, with the constraint $\Sigma_k \mu_k = 0$. Note that larger μ_h and μ_i values indicate better performance of the method applied on images h and i, respectively. This analysis retrieved estimated values and standard errors of four performance indicators corresponding to the image quality of the proposed method, TV denoising, BM3D, and ground truth. We used package ordBTL[18] implemented in R to fit the model. We performed Wald tests with Bonferroni correction

to test the null hypotheses that there was no significant difference between μ_h and μ_i. Inter-rater agreement was assessed with kappa statistics based on squared disagreement weights.

Results

Acquisition and computation time

The acquisition time using NEX 9 with b = 1000 s/mm^2 and NEX 1 with b = 0 s/mm^2 was approximately 5 min 20 s, whereas that using NEX 1 for both b values of 1000 and 0 s/mm^2, corresponding to the case when using the proposed CNN-based method, was 50 s. We performed the calculations on a PC with Intel Core-i7 8700K CPU and a Nvidia Geforce GTX 1080 Ti graphics processing unit. The proposed method was the post-processing after reconstruction. The resulting computation time per slice for our post-processing was 1.9 ms, being negligible compared to the computation time for reconstruction.

Diffusion-weighted image quality

The average peak SNR results obtained from applying the evaluated methods on the images and that of pre-denoising images in the test set are listed in Table 1. Paired t-tests with Bonferroni correction show that the proposed method significantly ($P < 0.001$) achieves higher peak SNRs than the other algorithms. Figure 3 shows an image from the test set and its processing results. The magnified image in Fig. 3h shows that the Gaussian filter does not suitably remove noise, and that in Fig. 3i shows that TV denoising achieves better performance but produces a patchy appearance by its piecewise constant assumption. In contrast, the magnified images obtained from BM3D (Fig. 3j) and the proposed method (Fig. 3k) exhibit the expected appearance. A closer inspection shows that the proposed CNN denoising is superior to BM3D in terms of reconstructing fine structures such as the sulci observed in the ground-truth image (Fig. 3l).

Table 1 Peak SNRs of diffusion-weighted images compared with the ground truth. The peak SNRs of pre-denoising images are also listed

Method	Peak SNR (dB)
Pre-denoising	31.33 (1.63)
Gaussian	34.23 (1.48)
TV	34.59 (1.50)
BM3D	34.95 (1.54)
Proposed	36.06 (1.54)

Standard deviations are enclosed in parentheses. SNR, signal-to-noise ratio; TV, total variation; BM3D, block-matching and 3D filtering.

Reader study

The results of the visual assessment performed by the two radiologists are summarized in Table 2. The weighted kappa statistics is 0.767, indicating excellent inter-rater agreement. The performance indicators of image quality (μ) are shown in Fig. 4. In both results, the ground truth retrieves the highest μ, followed by the proposed method. Our approach significantly outperforms the other denoising algorithms, TV and BM3D. The ranks of the performance indicators are consistent with the peak SNR values.

Discussion

We perform denoising using a deep neural network and multi-shot EPI sequence to obtain high-resolution diffusion-weighted images of the brain in < 1 min. The acquisition time is short enough to allow high-resolution DWI to be used in daily clinical practice. The CNN processing also requires low computational cost, being suitable to be implemented on commercial scanners. The proposed fast and high-resolution DWI retrieved the highest quality in both quantitative and

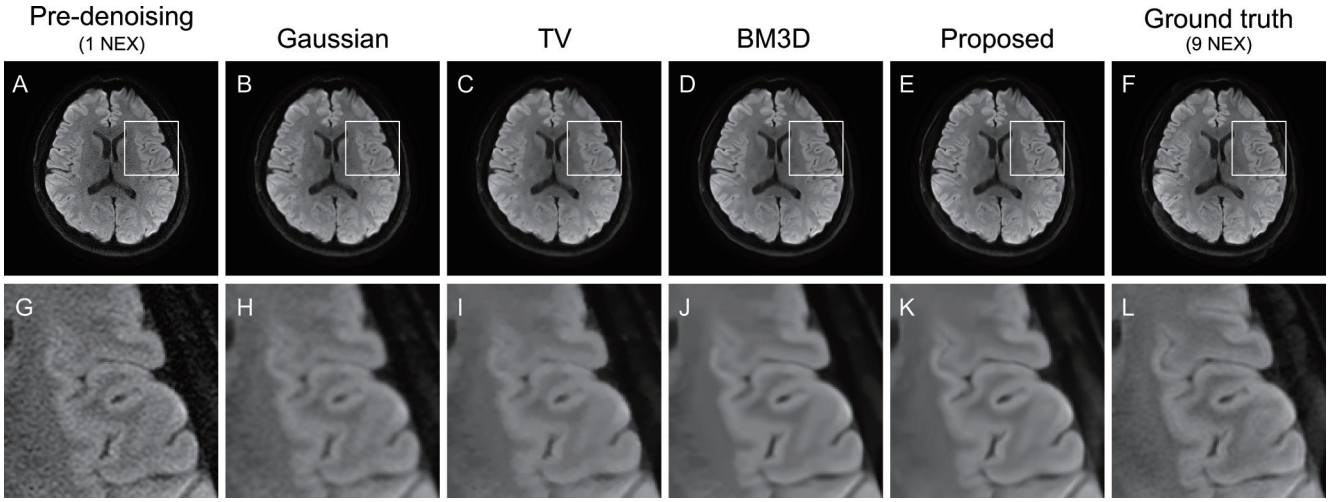

Fig. 3 Pre-denoising, denoised, and ground truth diffusion-weighted images. (**A**) Pre-denoising image. Images denoised using (**B**) Gaussian filter, (**C**) total variation (TV) denoising, (**D**) block-matching and 3D filtering (BM3D), and (**E**) the proposed method. (**F**) Ground truth images. (**G**–**I**) Magnified images of the solid boxes in (**A**–**F**), respectively.

Table 2 Comparison among image pairs from reader study

Pair (*h*, *i*)	Reader 1					Reader 2				
	h is much better	*h* is better	No preference	*i* is better	*i* is much better	*h* is much better	*h* is better	No preference	*i* is better	*i* is much better
TV, BM3D	0	0	1	18	0	0	0	0	0	19
TV, proposed	0	0	0	15	4	0	0	0	0	19
TV, ground truth	0	0	0	0	19	0	0	0	0	19
BM3D, proposed	0	1	5	11	2	0	1	7	9	2
BM3D, ground truth	0	1	4	9	5	0	4	3	12	0
Proposed, ground truth	0	3	5	10	1	0	6	3	10	0

TV, total variation; BM3D, block-matching and 3D filtering.

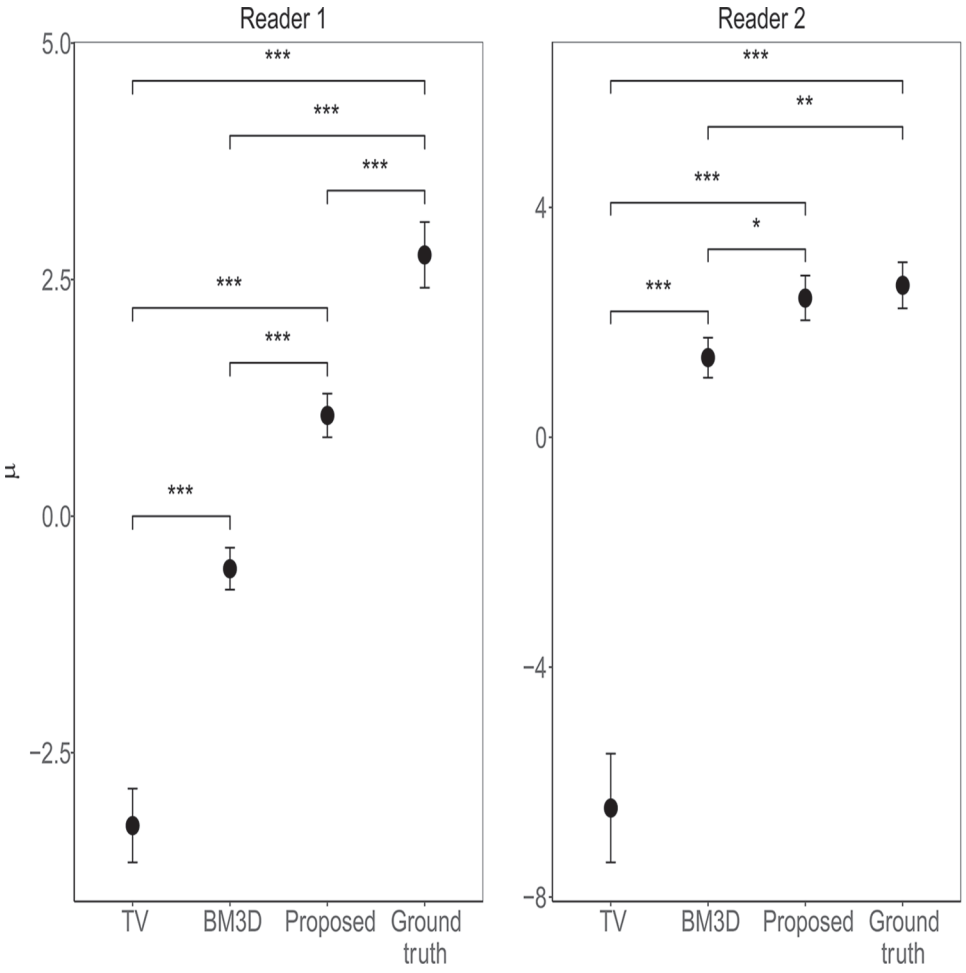

Fig. 4 Estimates of variable μ for cumulative logit model fitted to paired comparison. μ represents image quality of the corresponding method or ground truth. Larger μ indicates better quality. Estimated asymptotic standard errors are denoted by error bars. TV, total variation; BM3D, block-matching and 3D filtering. The significance stars mean: $^{*}P < 0.05$; $^{**}P < 0.01$; $^{***}P < 0.001$.

qualitative evaluations among the evaluated denoising methods. This illustrates that our approach can minimize deterioration of image quality and diagnostic accuracy arising from fast acquisition without signal averaging. Despite its superiority over the conventional methods, the quality of the images denoised by the proposed method was judged worse than that of ground truth by one reader. He pointed out that the proposed method slightly obscured the anatomical structure of the basal ganglia and the border between white and gray matter. This subtle change cannot be captured well by the peak SNR, which mainly depends on noise level. More improvement in preserving fine structures is the subject of our future research. It is also noted that multi-shot EPI combined with parallel imaging is prone to aliasing by an unfolding algorithm with inappropriate reconstruction parameters. Mild aliasing artifacts may appear even

in the ground truth images under our setting where two-shot multiplexed sensitivity encoding is used along with parallel imaging with reduction factor of 2. Our current approach has difficulty in solving the problem because the CNN learns to imitate ground truth data. However, aliasing can be reduced by more sophisticated reconstructions such as an algorithm based on low-rank Hankel matrix completion.[19] Although the algorithm is time-consuming, its high computational cost can be mitigated using CNNs.[20] The incorporation of it into our approach could enable the removal of both noise and aliasing.

Diffusion-weighted imaging currently conforms a routine protocol for brain MRI given its high contrast resolution. Although combining EPI and DWI has drawbacks including limited spatial resolution and image distortion, they are overcome by the high contrast resolution that is valuable for clinical evaluation, especially for acute brain ischemia. During the past decade, DWI has been adopted in body MR protocols for screening and diagnosis of the malignant lesions[21] and quantitative assessments.[22,23] To prevent image distortion caused by high image resolution in EPI-based sequences, various methods for acquisition of high-resolution DWI have been developed and tested.[6,7,24–26] These techniques, however, exhibit a limited SNR in a small voxel, thus demanding multiple averaging that consequently increases the acquisition time.

To achieve high-resolution DWI in a shorter acquisition time, imaging with noise suppression or effective signal acquisition can be used. Noise reduction using deep neural networks has been developed for general image processing[27] and can be applied for accelerated MRI acquisition. Some studies have addressed the acceleration of MRI by incorporating deep neural networks into reconstruction.[28–30] These works focused on various *k*-space under-sampling schemes to remove artifacts related to under-sampling by using learning-based methods. Image acquisition can be accelerated by reducing the sampling rate in, for example, fast spin-echo imaging. However, DWI is usually combined with EPI to collect all the points on a *k*-space with a single-pulse excitation, essentially receiving no benefit from the *k*-space under-sampling. In contrast, the proposed method prevents averaging to improve the SNR, being adequate for accelerating high-resolution DWI. More recent studies applied deep learning-based denoising to DWI.[31,32] But these works were limited to single-shot EPI, being susceptible to image distortion resulting from phase error in high-resolution. Note that multi-shot EPI is crucial to achieving both high-resolution and low distortion simultaneously. To the best of our knowledge, this study is the first attempt to combine a deep neural network-based denoising with multi-shot EPI to obtain high-resolution DWI.

Despite the promising preliminary results, the proposed method has several limitations. First, although the peak SNR is often used to evaluate the image quality, the relation between the peak SNR and diagnostic quality has not been thoroughly investigated in medical imaging. In this work, we conducted the reader study to complement the evaluation. In future work, we plan to make a more extensive visual assessment including image sharpness. Second, our experiments relied on data from a very limited number of subjects. Further evaluation on more test data is necessary, and a more extensive evaluation of image quality should be performed considering both anatomy and pathology.

Conclusion

We propose a denoising method using deep neural networks to acquire high-resolution diffusion weighted images based on multi-shot EPI with shorter scan times than other methods. We experimentally verified the superior quality of the proposed method compared with conventional techniques, including the state-of-the-art TV denoising and BM3D, in both quantitative and qualitative assessments. The results indicate the potential of deep learning to dramatically reduce the acquisition time and improve the quality of high-resolution DWI.

Conflicts of Interest

Dr. Onishi received the patent royalty for Abches from Apex Medical and research funding from Accuray Japan and Ono Pharmacy. None of the other authors declare any conflict of interest.

References

1. Moseley ME, Kucharczyk J, Mintorovitch J, et al. Diffusion-weighted MR imaging of acute stroke: correlation with T2-weighted and magnetic susceptibility-enhanced MR imaging in cats. AJNR Am J Neuroradiol 1990; 11:423–429.
2. Stehling MK, Turner R, Mansfield P. Echo-planar imaging: magnetic resonance imaging in a fraction of a second. Science 1991; 254:43–50.
3. Wu W, Miller KL. Image formation in diffusion MRI: a review of recent technical developments. J Magn Reson Imaging 2017; 46:646–662.
4. Pruessmann KP, Weiger M, Scheidegger MB, Boesiger P. SENSE: sensitivity encoding for fast MRI. Magn Reson Med 1999; 42:952–962.
5. Griswold MA, Jakob PM, Heidemann RM, et al. Generalized autocalibrating partially parallel acquisitions (GRAPPA). Magn Reson Med 2002; 47:1202–1210.
6. Porter DA, Heidemann RM. High resolution diffusion-weighted imaging using readout-segmented echo-planar imaging, parallel imaging and a two-dimensional navigator-based reacquisition. Magn Reson Med 2009; 62:468–475.
7. Chen NK, Guidon A, Chang HC, Song AW. A robust multi-shot scan strategy for high-resolution diffusion weighted MRI enabled by multiplexed sensitivity-encoding (MUSE). Neuroimage 2013; 72:41–47.
8. LeCun Y, Bengio Y, Hinton G. Deep learning. Nature 2015; 521:436–444.
9. Krizhevsky A, Sutskever I, Hinton GE. Imagenet classification with deep convolutional neural networks. In: Pereira F, Burges C, Bottou L, Weinberger K, eds. Advances in

neural information processing systems, vol. 25. New York: Curran Associates, Inc., 2012; 1106–1114.
10. He K, Zhang X, Ren S, Sun J. Deep residual learning for image recognition. Proceedings of the IEEE Conference on Computer Vision and Pattern Recognition (CVPR). Las Vegas, NV, USA: IEEE, 2016; 770–778.
11. Zhang K, Zuo W, Chen Y, Meng D, Zhang L. Beyond a Gaussian denoiser: residual learning of deep CNN for image denoising. IEEE Trans Image Process 2017; 26:3142–3155.
12. Kingma DP, Ba J. Adam: A method for stochastic optimization. 2014 arXiv preprint arXiv:1412.6980.
13. Rudin LI, Osher S, Fatemi E. Nonlinear total variation based noise removal algorithms. Phys D 1992; 60:259–268.
14. Dabov K, Foi A, Katkovnik V, Egiazarian K. Image denoising by sparse 3-D transform-domain collaborative filtering. IEEE Trans Image Process 2007; 16:2080–2095.
15. Goldstein T, Osher S. The split Bregman method for L1-regularized problems. SIAM J Imaging Sci 2009; 2:323–343.
16. Agresti A. Analysis of ordinal paired comparison data. J Royal Stat Soc Ser C Appl Stat 1992; 41:287–297.
17. Agresti A. Categorical data analysis, 2nd ed. New York: Wiley, 2002; 267–313.
18. Casalicchio G. ordBTL: modelling comparison data with ordinal response. Available from: https://cran.r-project.org/web/packages/ordBTL/index.html (Accessed 10 August, 2018).
19. Mani M, Jacob M, Kelley D, Magnotta V. Multi-shot sensitivity-encoded diffusion data recovery using structured low-rank matrix completion (MUSSELS). Magn Reson Med 2017; 78:494–507.
20. Aggarwal HK, Mani MP, Jacob M. MoDL-MUSSELS: model-based deep learning for multishot sensitivity-encoded diffusion MRI. IEEE Trans Med Imaging 2019. doi: 10.1109/TMI.2019.2946501.
21. Eiber M, Holzapfel K, Ganter C, et al. Whole-body MRI including diffusion-weighted imaging (DWI) for patients with recurring prostate cancer: technical feasibility and assessment of lesion conspicuity in DWI. J Magn Reson Imaging 2011; 33:1160–1170.
22. Manning P, Murphy P, Wang K, et al. Liver histology and diffusion-weighted MRI in children with nonalcoholic fatty liver disease: a MAGNET study. J Magn Reson Imaging 2017; 46:1149–1158.
23. Ichikawa S, Motosugi U, Hernando D, et al. Histological grading of hepatocellular carcinomas with intravoxel incoherent motion diffusion-weighted imaging: inconsistent results depending on the fitting method. Magn Reson Med Sci 2018; 17:168–173.
24. Dong Z, Wang F, Reese TG, et al. Tilted-CAIPI for highly accelerated distortion-free EPI with point spread function (PSF) encoding. Magn Reson Med 2019; 81:377–392.
25. Wen Q, Kodiweera C, Dale BM, Shivraman G, Wu YC. Rotating single-shot acquisition (RoSA) with composite reconstruction for fast high-resolution diffusion imaging. Magn Reson Med 2018; 79:264–275.
26. Yamaguchi K, Nakazono T, Egashira R, et al. Diagnostic performance of diffusion tensor imaging with readout-segmented echo-planar imaging for invasive breast cancer: correlation of ADC and FA with pathological prognostic markers. Magn Reson Med Sci 2017; 16:245–252.
27. Xie J, Xu L, Chen E. Image denoising and inpainting with deep neural networks. In: Pereira F, Burges C, Bottou L, Weinberger K, eds. Advances in neural information processing systems, vol. 25. New York: Curran Associates, Inc., 2012; 341–349.
28. Hammernik K, Klatzer T, Kobler E, et al. Learning a variational network for reconstruction of accelerated MRI data. Magn Reson Med 2018; 79:3055–3071.
29. Han Y, Yoo J, Kim HH, Shin HJ, Sung K, Ye JC. Deep learning with domain adaptation for accelerated projection-reconstruction MR. Magn Reson Med 2018; 80:1189–1205.
30. Eo T, Jun Y, Kim T, Jang J, Lee HJ, Hwang D. KIKI-net: cross-domain convolutional neural networks for reconstructing undersampled magnetic resonance images. Magn Reson Med 2018; 80:2188–2201.
31. Wang H, Zheng R, Dai F, Wang Q, Wang C. High-field MR diffusion-weighted image denoising using a joint denoising convolutional neural network. J Magn Reson Imaging 2019; 50:1937–1947.
32. Kidoh M, Shinoda K, Kitajima M, et al. Deep learning based noise reduction for brain MR imaging: tests on phantoms and healthy volunteers. Magn Reson Med Sci 2020; 19:195–206.